Fock-space relativistic coupled-cluster calculations of clock-transition properties in Pb^{2+}

Palki Gakkhar,[1] Ravi Kumar,[2] D. Angom,[3] and B. K. Mani[1,*]
[1]*Department of Physics, Indian Institute of Technology, Hauz Khas, New Delhi 110016, India*
[2]*Department of Chemistry, University of Zurich, 8057 Zurich, Switzerland*
[3]*Department of Physics, Manipur University, Canchipur 795003, Manipur, India*

(Received 13 April 2024; accepted 1 July 2024; published 22 July 2024)

We implement an all-particle multireference Fock-space relativistic coupled-cluster theory to probe the $6s^2\,{}^1S_0$–$6s6p\,{}^3P_0^o$ clock transition in an even isotope of Pb^{2+}. We compute the excitation energy for several low-lying states, $E1$ and $M1$ transition amplitudes, and the lifetime of the clock state. Moreover, we also calculate the ground-state dipole polarizability using perturbed relativistic coupled-cluster theory. To improve the accuracy of results, we incorporate the corrections from the relativistic and QED effects in all our calculations. The contributions from triple excitations are accounted perturbatively. Our computed excitation energies are in excellent agreement with the experimental values for all the states. Our result for lifetime, 9.76×10^6 s, of clock state is approximately 8.5% larger than the previous value using a combined method of configuration-interaction and many-body perturbation theory [Phys. Rev. Lett. **127**, 013201 (2021)]. Based on our analysis, we find that the contributions from the valence-valence correlations arising from higher-energy configurations and the corrections from the perturbative triples and QED effects are essential to get accurate clock transition properties in Pb^{2+}. Our computed value of dipole polarizability is in good agreement with the available theoretical and experimental data.

DOI: 10.1103/PhysRevA.110.013119

I. INTRODUCTION

Optical atomic clocks are one of the most accurate time measurement instruments in existence today [1,2]. Due to their unprecedented accuracies as frequency and time standards, they can serve as important probes of fundamental phenomena in physics and function as key components in technological applications. Some examples where atomic clocks are of vital importance include measuring the variation in fundamental constants [3–5], probing physics beyond the standard model of particle physics [6,7], navigation systems [8,9], quantum computers [10,11], the basis for redefining the second [5,12], and others [1,2]. For the single-ion optical clocks, the hyperfine-induced $3s^2\,{}^1S_0$–$3s3p\,{}^3P_0^o$ (267.4 nm) transition based $^{27}Al^+$ is demonstrated to be one of the best clocks, with a fractional frequency uncertainty of 9.4×10^{-19} [13]. The high accuracy in $^{27}Al^+$ could be attributed to the low sensitivity to electromagnetic fields, narrow natural linewidth, and small room-temperature blackbody radiation (BBR) shift in the clock transition frequency [14–16]. Among the neutral atoms, a lattice clock based on degenerate fermionic ^{87}Sr atoms with a hyperfine-induced $5s^2\,{}^1S_0$–$5s5p\,{}^3P_0^o$ (698 nm) transition is reported to be one of the best neutral atom clocks. The smallest fractional frequency error achieved is approximately equal to 2.0×10^{-18} [17,18].

In the quest for a new and improved frequency standard, an optical clock based on the $6s^2\,{}^1S_0$–$6s6p\,{}^3P_0^o$ transition, mediated through a two-photon $E1 + M1$ channel, in a doubly ionized even isotope of lead (Pb^{2+}) could be a promising candidate. Like in $^{27}Al^+$, the clock transition is an electric-dipole-forbidden transition between two $J = 0$ states, providing a strong resistance to the environmental perturbations. In addition, unlike $^{27}Al^+$, the nuclear spin quantum number I is zero. This is crucial, as it prevents clock transition from the nonscalar perturbations which may arise through the coupling between the electron and nuclear multipole moments. Despite this important prospect with Pb^{2+} as an accurate optical atomic clock, the properties of the relevant transition have not been explored in detail. For example, in terms of theoretical calculations, we are aware of only one study on the lifetime of the clock state [19]. The work [19], employing a combined configuration-interaction (CI) and many-body perturbation theory (MBPT) method, computed the lifetime τ of the clock state $^3P_0^o$ as 9.0×10^6 s. Considering that there are no experimental data, additional theoretical calculations, especially using the accurate methods such as the relativistic coupled-cluster (RCC) method, would be crucial to get better and accurate insights into the clock properties. Moreover, the inclusion of relativistic and QED corrections in the calculations of properties is essential to obtain reliable results. It can thus be concluded that there is a clear gap in the research in terms of the scarcity of results for accurate properties of the $^1S_0$-$^3P_0^o$ clock transition of Pb^{2+}.

In this work we implement an all-particle multireference Fock-space relativistic coupled-cluster (FSRCC) theory to compute the clock transition properties of Pb^{2+} accurately. It should be noted that the RCC theory is one of the most reliable quantum many-body theories for atomic structure calculations. It accounts for electron correlation effects to all orders of residual Coulomb interaction and has been employed to obtain accurate results in several closed-shell and one-valence

*Contact author: bkmani@physics.iitd.ac.in

atoms and ions [20–23]. The application of the RCC theory for two-valence atomic systems, such as the present case of Pb^{2+} clock transition, however, is limited to a few studies [24–26]. The reason for this is perhaps the complications associated with the implementation of the FSRCC theory for multireference systems [16,24–26]. To address the clock transition properties in a comprehensive way, using the FSRCC theory [16,26], we carry out precise calculations of the excitation energies and $E1$ and $M1$ transition amplitudes associated with the $^1S_0$-$^3P_0^o$ transition in Pb^{2+}. Using these results, we then calculate the lifetime of the $^3P_0^o$ clock state. In addition, as electric dipole polarizability is a crucial parameter for estimating the BBR shift in clock frequency, we also calculate the ground-state polarizability of Pb^{2+} using perturbed relativistic coupled-cluster (PRCC) theory [23,27]. Moreover, in all these calculations of properties, we incorporate and analyze the contributions from the Breit interaction, QED corrections, and perturbative triples.

The remainder of the paper is organized as follows. In Sec. II we provide a brief description of the FSRCC theory for two-valence atomic systems. We give the coupled-cluster working equation for two-valence systems. In Sec. III we provide and discuss the expression for the $E1M1$ decay rate. The results obtained from our calculations are presented and analyzed in Sec. IV. Theoretical uncertainty in our computed results is discussed in Sec. V. We summarize in Sec. VI. Unless stated otherwise, all results and equations presented in this paper are in atomic units ($\hbar = m_e = e = 1/4\pi\epsilon_0 = 1$).

II. TWO-VALENCE FSRCC THEORY

Since the clock transition in Pb^{2+} involves atomic state functions of two-valence nature, we need an accurate multireference theory to calculate these wave functions and corresponding many-body energies. In the present work we employ a FSRCC theory for two valence [16,26] to obtain the many-body wave function and corresponding energy. In Refs. [16,26,28], we discussed in detail the implementation of FSRCC theory in the form of sophisticated parallel codes and also gave the working equations and Goldstone diagrams contributing to the theory. So here, for completeness, we provide a very brief description of the FSRCC theory for two-valence atoms and calculations of properties using it in the context of Pb^{2+}.

The atomic state function for a two-valence atom or ion is obtained by solving the many-body Schrödinger equation

$$H^{\rm DCB}|\Psi_{vw}\rangle = E_{vw}|\Psi_{vw}\rangle, \tag{1}$$

where $|\Psi_{vw}\rangle$ is the exact many-body wave function and E_{vw} is the corresponding exact energy; the indices v and w represent the valence orbitals; and $H^{\rm DCB}$ is the Dirac-Coulomb-Breit no-virtual-pair Hamiltonian used in all calculations, expressed as

$$H^{\rm DCB} = \sum_{i=1}^{N}[c\boldsymbol{\alpha}_i\cdot\mathbf{p}_i + (\beta_i - 1)c^2 - V_N(r_i)] + \sum_{i<j}\left(\frac{1}{r_{ij}} + g^{\rm B}(r_{ij})\right), \tag{2}$$

where $\boldsymbol{\alpha}$ and β are the Dirac matrices and $1/r_{ij}$ and $g^{\rm B}(r_{ij})$ are the Coulomb and Breit interactions, respectively. In the FSRCC theory, $|\Psi_{vw}\rangle$ is written as

$$|\Psi_{vw}\rangle = e^T\left[1 + S_1 + S_2 + \tfrac{1}{2}\left({S_1}^2 + {S_2}^2\right) + R_2\right]|\Phi_{vw}\rangle, \tag{3}$$

where $|\Phi_{vw}\rangle = a_w^\dagger a_v^\dagger|\Phi_0\rangle$ is the Dirac-Fock reference state for a two-valence system; operators T, S, and R are the electron excitation operators, referred to as the coupled-cluster (CC) operators, for closed-shell, one-valence, and two-valence sectors, respectively; and the subscripts 1 and 2 with these operators represent the single and double excitations, referred to as the coupled-cluster with singles and doubles (CCSD) approximation. The FSRCC theory with CCSD approximation subsumes most of the electron correlation effects in atomic structure calculations and provides an accurate description of the calculated properties. In the second quantized representation, the CC operators are expressed as

$$T_1 = \sum_{ap} t_a^p a_p^\dagger a_a, \quad T_2 = \frac{1}{2!}\sum_{abpq} t_{ab}^{pq} a_p^\dagger a_q^\dagger a_b a_a, \tag{4a}$$

$$S_1 = \sum_{p} s_v^p a_p^\dagger a_v, \quad S_2 = \sum_{apq} s_{va}^{pq} a_p^\dagger a_q^\dagger a_a a_v, \tag{4b}$$

$$R_2 = \sum_{pq} r_{vw}^{pq} a_p^\dagger a_q^\dagger a_w a_v. \tag{4c}$$

Here the indices $a, b, \ldots$ and $p, q, \ldots$ represent the core and virtual orbitals, respectively, and $t_{\cdots}^{\cdots}$, $s_{\cdots}^{\cdots}$, and $r_{\cdots}^{\cdots}$ are the cluster amplitudes corresponding to T, S, and R coupled-cluster operators, respectively. The diagrammatic representation of these operators is shown in Fig. 1. It should however be mentioned that the dominant contributions from triple excitations are also included using the approach of perturbative triples [16].

The operators for closed-shell and one-valence sectors are obtained by solving the set of coupled nonlinear equations discussed in Refs. [21,29], respectively. The two-valence CC operator R_2 is obtained by solving the CC equation [16,26]

$$\left\langle\Phi_{vw}^{pq}\middle|\bar{H}_{\rm N} + \{\bar{H}_{\rm N}S'\} + \{\bar{H}_{\rm N}R_2\}\right|\Phi_{vw}\rangle = E_{vw}^{\rm att}\left\langle\Phi_{vw}^{pq}\middle|[S' + R_2]\right|\Phi_{vw}\rangle. \tag{5}$$

Here, for compact notation, we use $S' = S_1 + S_2 + \frac{1}{2}(S_1^2 + S_2^2)$. In addition, $E_{vw}^{\rm att}$ is the two-electron attachment energy, which is expressed as the difference between the correlated energy of the $(n-2)$-electron (closed-shell) and n-electron (two-valence) sectors $E_{vw} - E_0$.

Figure 2 shows the Goldstone diagrams contributing to the linearized FSRCC theory for two-valence systems. These are obtained by considering the terms with only one order of CC operators in Eq. (5) and then contracting the residual Coulomb interaction with these CC operators using Wick's theorem. The CC diagrams in Figs. 2(l)–2(n) are referred to as the folded diagrams and they arise due to renormalization terms on the right-hand side of Eq. (5). The presence of folded diagrams in open-shell systems constitutes one of the main differences from the CC theory of closed-shell systems. The rectangular portion represents the effective energy diagrams arising from the one-valence [Fig. 2(l)] and two-valence

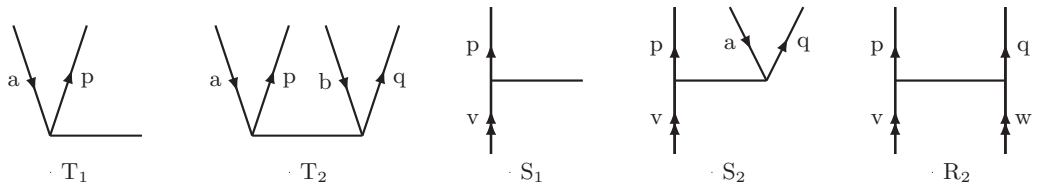

FIG. 1. Diagrammatic representation of closed-shell, one-valence, and two-valence single and double CC operators.

[Figs. 2(m) and 2(n)] sectors. The Goldstone diagrams in Fig. 2 correspond to the algebraic expression

$$\begin{aligned}&\langle H_{\rm N}\rangle_{vw}^{pq} + \langle \overbrace{H_{\rm N}T}\rangle_{vw}^{pq} + \langle \overbrace{H_{\rm N}S'}\rangle_{vw}^{pq} + \langle \overbrace{H_{\rm N}R_2}\rangle_{vw}^{pq}\\ &- \langle \overbrace{E_{vw}^{\rm att}S'}\rangle_{vw}^{pq} - \langle \overbrace{E_{vw}^{\rm att}R_2}\rangle_{vw}^{pq} = g_{pqvw} + g_{pqrw}s_v^r\\ &- g_{aqvw}t_a^p + \tilde{g}_{pavr}s_{aw}^{rq} + g_{pqvw}\epsilon_p + g_{pqrs}r_{vw}^{rs}\\ &- g_{aqvr}s_{aw}^{pr} + g_{abvw}t_{ab}^{pq} - g_{aqrw}s_{va}^{rp} - E_w^{\rm att}r_{vw}^{pq}\\ &- E_{vw}^{\rm att}s_v^p - E_{vw}^{\rm att}r_{vw}^{pq},\end{aligned} \tag{6}$$

where $\tilde{g}_{ijkl} = g_{ijkl} - g_{ijlk}$. Since we use Dirac-Fock orbitals in our calculations, Fig. 2(f) does not contribute and therefore is not included in the expression.

III. $E1M1$ DECAY RATE USING FSRCC THEORY

Since $I = J = F = 0$ for the $^1S_0$-$^3P_0^o$ clock transition in Pb^{2+}, it is allowed through a two-photon $E1 + M1$ channel. As shown in the schematic diagram in Fig. 3, in the first route, the initial state $|\Psi_i\rangle$ can couple to a same-parity state through a magnetic dipole operator (photon with energy ω_1) and then connect to the final state $|\Psi_f\rangle$ through an electric dipole operator (photon with energy ω_2). Alternatively, in the second route, the initial state $|\Psi_i\rangle$ can couple to an opposite-parity state via an electric dipole operator first and then connect to the ground state through a magnetic dipole operator. Mathematically, the $E1 + M1$ decay rate from $|\Psi_f\rangle$ to $|\Psi_i\rangle$ can be expressed in terms of the reduced matrix elements of electric and magnetic dipole operators as [30,31]

$$\begin{aligned}\Gamma_{E1M1} = \frac{8}{27\pi}\alpha^6 \int_0^\infty d\omega_1\omega_1^3 \int_0^\infty d\omega_2\omega_2^3\\ \times \left| \sum_n \frac{\langle\Psi_f||\mathbf{D}||\Psi_n\rangle\langle\Psi_n||M_1||\Psi_i\rangle}{E_n + \omega_1 - E_i}\right.\\ \left. + \sum_{\bar{n}} \frac{\langle\Psi_f||M_1||\bar{\Psi}_n\rangle\langle\bar{\Psi}_n||\mathbf{D}||\Psi_i\rangle}{E_{\bar{n}} + \omega_2 - E_i}\right|^2\\ \times \delta(E_i + \omega_1 + \omega_2 - E_f).\end{aligned} \tag{7}$$

Here, for Pb^{2+}, $|\Psi_i\rangle = 6s6p\,^3P_0^o$, $|\Psi_f\rangle = 6s^2\,^1S_0$, $|\Psi_n\rangle = 6s6p\,^3P_1^o, 6s6p\,^1P_1^o$, and $|\bar{\Psi}_n\rangle = 6s7s\,^3S_1, 6s6d\,^3D_1$. Since the transition is allowed through two photons, the energy difference between final and initial states satisfies the relation $E_f - E_i = \omega_1 + \omega_2$. Additionally, since all intermediate states $^3P_1^o$, $^1P_1^o$, $^3S_1$, and $^3D_1$ have energy higher than that of $^3P_0^o$, the decay rate equation will not exhibit any poles.

The reduced matrix elements in Eq. (7) are calculated using the FSRCC theory. The calculation of properties using the FSRCC theory is explained in detail in Ref. [16]. However, to illustrate it briefly in the present work, we consider the example of dipole matrix elements. Using the RCC wave function from Eq. (3), the dipole matrix elements is

$$\begin{aligned}\langle\Psi_f|\mathbf{D}|\Psi_n\rangle = \sum_{kl} c_k^{f*}c_l^n[\langle\Phi_k|\tilde{\mathbf{D}} + \tilde{\mathbf{D}}(S' + R_2) + (S' + R_2)^\dagger\tilde{\mathbf{D}}\\ + (S' + R_2)^\dagger\tilde{\mathbf{D}}(S' + R_2)|\Phi_l\rangle],\end{aligned} \tag{8}$$

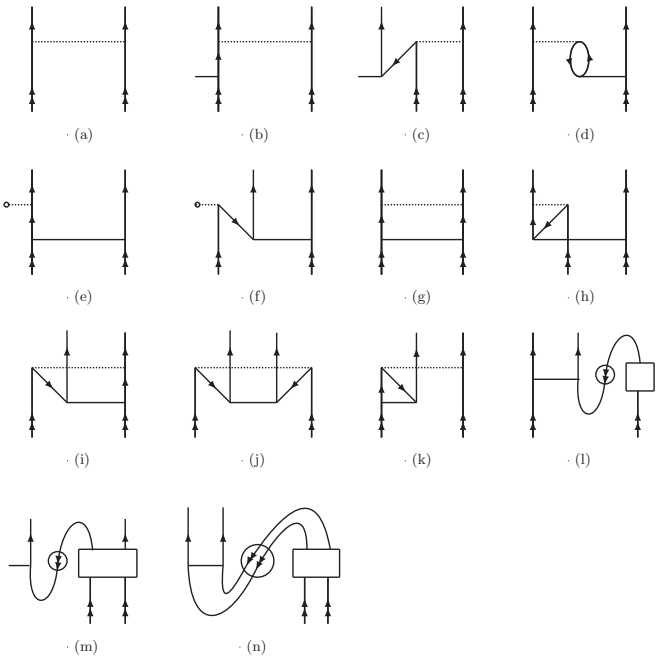

FIG. 2. The CC diagrams contributing to the linearized FSRCC theory for two-valence atomic systems. Diagrams (l)–(n) are referred to as the folded diagrams and arise from the renormalization terms in CC equations for multireference systems.

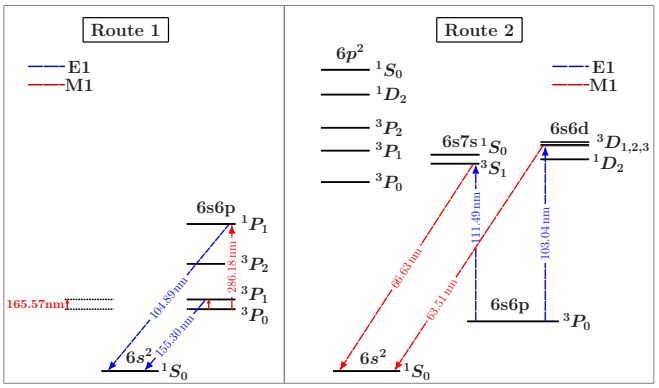

FIG. 3. Schematic energy-level diagram for the $6s^2\,^1S_0 \rightarrow 6s6p\,^3P_0^o$ clock transition in Pb^{2+} via a two-photon $E1 + M1$ transition.

where the coefficients c_k^f represent the mixing coefficients in the expansion of a multireference configuration state function $|\Phi_f\rangle$. These are obtained by diagonalizing the $H^{\rm DCB}$ matrix within the chosen model space. The dressed operator $\tilde{\mathbf{D}} = e^{T^\dagger}\mathbf{D}e^T$ is a nonterminating series in the closed-shell CC operator T. Including all orders of T in the dressed operator is practically challenging. In Ref. [29] an algorithm was developed to include a class of dominant diagrams to all orders in T, iteratively, in the dressed Hamiltonian. Based on this study, we concluded that the terms higher than quadratic in T contribute less than 0.1% to the properties. So in the present work we truncate $\tilde{\mathbf{D}}$ after the second order in T and include the $\tilde{\mathbf{D}} \approx \mathbf{D} + \mathbf{D}T + T^\dagger\mathbf{D} + T^\dagger\mathbf{D}T$ terms in the calculation of properties.

IV. RESULTS AND DISCUSSION

A. Single-particle basis and convergence of properties

An accurate description of single-electron wave functions and corresponding energies is crucial to obtain the reliable results using the FSRCC theory. In the present work we use the Gaussian-type orbitals (GTOs) [32] as the single-electron basis for FSRCC calculations. The GTOs are used as the finite basis sets in which the single-electron wave functions are expressed as a linear combination of the Gaussian-type functions (GTFs). More precisely, the GTFs of the large component of the wave function are expressed as

$$g_{\kappa p}^L(r) = C_{\kappa i}^L r^{n_\kappa} e^{-\alpha_p r^2}, \tag{9}$$

where $p = 0, 1, 2, \ldots, N$ is the GTO index, with N the total number of GTFs. The exponent α_p is further expressed as $\alpha_0\beta^{p-1}$, where α_0 and β are the two independent parameters. The parameters α_0 and β are optimized separately for each orbital symmetry so that the single-electron wave functions and energies match well with the numerical values obtained from the GRASP2K [33]. The small components of wave functions are derived from the large components using the kinetic balance condition [34].

In Table I we provide the optimized values of α_0 and β parameters for Pb^{2+} and compare the values of single-electron and self-consistent field (SCF) energies with GRASP2K [33] and B-spline [35] results. It should be mentioned that the single-electron basis used in the calculations of properties also incorporates the effects of Breit interaction, vacuum polarization, and self-energy corrections. As evident from the table, the single-particle and SCF energies are in excellent agreement with GRASP2K and B-spline results. The largest differences at the level of SCF and single-particle energies are 0.0001% and 0.0003%, respectively.

Since GTOs are a mathematically incomplete basis, convergence of the properties results with basis size must be checked to get reliable results using the FSRCC method. To show the convergence of results, in Table II we list the values of electric dipole polarizability and $E1$ and $M1$ transition reduced matrix elements with increasing basis size. To obtain a converged basis, we start with a moderate basis size and add orbitals systematically to each symmetry until the change in the properties is less than or equal to 10^{-3} in respective units. For example, as evident from the table, the change in $E1$ amplitude of the $\langle {}^1S_0||D||{}^1P_1^o\rangle$ transition is of the order of 10^{-3} a.u. when the basis is augmented from 158 ($24s21p18d13f8g7h$) to 169 ($25s22p19d14f9g8h$) orbitals. So to minimize the computation time, we consider the basis set with 169 orbitals as optimal and use it for further FSRCC calculations where the corrections from the Breit interaction, vacuum polarization, and self-energy are incorporated.

TABLE I. Single-particle and SCF energies (in a.u.) from GTOs compared with GRASP2K and B-spline results. The optimized α_0 and β parameters for the even-tempered basis used in our calculations are also provided.

Orbital	GTO	GRASP2K	B-spline
$1s_{1/2}$	−3257.41150	−3257.40298	−3257.41571
$2s_{1/2}$	−589.39795	−589.39605	−589.39835
$2p_{1/2}$	−565.00395	−565.00364	−565.00295
$2p_{3/2}$	−484.41530	−484.41512	−484.41548
$3s_{1/2}$	−145.26466	−145.26400	−145.26472
$3p_{1/2}$	−134.31668	−134.31639	−134.31638
$3p_{3/2}$	−116.10663	−116.10639	−116.10665
$3d_{3/2}$	−98.32473	−98.32446	−98.32473
$3d_{5/2}$	−94.48445	−94.48420	−94.48445
$4s_{1/2}$	−35.49304	−35.49280	−35.49305
$4p_{1/2}$	−30.72284	−30.72269	−30.72276
$4p_{3/2}$	−26.20738	−26.20725	−26.20737
$4d_{3/2}$	−18.43141	−18.43130	−18.43141
$4d_{5/2}$	−17.57859	−17.57861	−17.57859
$4f_{5/2}$	−7.44501	−7.44494	−7.44502
$4f_{7/2}$	−7.25330	−7.25331	−7.25331
$5s_{1/2}$	−7.63856	−7.63855	−7.63857
$5p_{1/2}$	−5.94459	−5.94458	−5.94458
$5p_{3/2}$	−5.09665	−5.09664	−5.09666
$5d_{3/2}$	−2.62373	−2.62373	−2.62373
$5d_{5/2}$	−2.51852	−2.51852	−2.51852
$E_{\rm SCF}$	−20910.40152	−20910.37469	−20910.40151
	α_0	β	GTOs
s	0.00450	1.805	40
p	0.00478	1.792	38
d	0.00605	1.855	34
f	0.00355	1.845	28

B. Excitation energy

The eigen energies obtained from the solution of the many-electron Schrödinger equation (1), using the FSRCC method, are used to calculate the excitation energies. The excitation energy of a general state $nln'l'\,{}^{(2S+1)}L_J$ is defined as

$$\Delta E_{nln'l'\,{}^{(2S+1)}L_J} = E_{nln'l'\,{}^{(2S+1)}L_J} - E_{ns^2\,{}^1S_0}, \tag{10}$$

where $E_{ns^2\,{}^1S_0}$ and $E_{nln'l'\,{}^{(2S+1)}L_J}$ are the exact energies of the ground and excited states, respectively. In Table III we list the excitation energies from our calculations along with other theoretical and experimental data for comparison. To account for valence-valence correlations more accurately, we also include $6p^2$, $6s6d$, and $6s7s$ configurations in the model space. For a quantitative assessment of electron correlations, we list the contributions from Breit and QED corrections separately.

TABLE II. Convergence trend of α, and $E1$ and $M1$ matrix elements as a function of basis size.

No. of orbitals	Basis	α	$\langle {}^1S_0 \|\|D\|\| {}^1P_1^o \rangle$	$\langle {}^3P_1^o \|\|M1\|\| {}^3P_0^o \rangle$
96	$20s15p12d7f4g0h$	15.919	2.0512	1.3158
103	$19s16p13d8f3g2h$	15.660	2.0268	1.3153
114	$20s17p14d9f4g3h$	14.979	1.9966	1.3198
125	$21s18p15d10f5g4h$	14.467	1.9873	1.3134
136	$22s19p16d11f6g5h$	14.274	1.9888	1.3126
147	$23s20p17d12f7g6h$	14.205	1.9883	1.3121
158	$24s21p18d13f8g7h$	14.175	1.9875	1.3118
169	$25s22p19d14f9g8h$	14.173	1.9854	1.3117

As evident from the table, our computed energies are in excellent agreement with the experimental results. The largest relative error in our calculation is approximately equal to 0.9%, which corresponds to the $^3P_0^o$ state. However, for other states, especially for those which contribute to the lifetime of the clock state, the errors are much smaller. The states $^3P_1^o$, $^1P_1^o$, $^3S_1$, and $^3D_1$, which couple either via the $E1$ or $M1$ operator in the clock transition, have relative errors of 0.06%, 0.13%, 0.07%, and −0.10%, respectively. This is crucial, as these energies contribute to the lifetime of the clock state. Among all the previous theoretical results listed in Table III, Ref. [37] is close to ours in terms of the many-body methods used, however, with an important difference. Reference [37] uses a linearized CCSD method, whereas the present work employs a nonlinear CCSD method, which accounts for electron correlation effects more accurately in the calculation. The relative errors in the reported excitation energies for $^3P_1^o$, $^1P_1^o$, $^3S_1$, and $^3D_1$ states in Ref. [37] are 1.08%, 0.53%, 0.73%, and 0.63%, respectively. The remaining results are mostly based on the multiconfiguration Hartree-Fock theory and its variations and in general are not consistent in terms of treating electron correlations.

Examining the contributions from high-energy configurations, we observe an improvement in the excitation energies of $^3P_1^o$ and $^1P_1^o$ states due to accounting for the valence-valence correlation more accurately. We find that the relative error reduces from 0.7% (0.6%) to 0.4% (0.3%) for the $^3P_1^o$ ($^1P_1^o$) state. Among the contributions from Breit interaction, vacuum

TABLE III. Two-electron removal energy of $^1S_0$ (cm^{-1}) and excitation energies of some low-lying excited states of Pb^{2+}. For quantitative analysis of electron correlations, contributions from Breit and QED corrections are given separately. Here DC denotes Dirac-Coulomb and VP denotes vacuum polarization.

States	DC-CCSD	Breit	Self-energy	VP	Total	Other calculations	NIST[a]	% error
$6s^2\,{}^1S_0$	599355.44	12.00	−0.67	188.97	599556	600984[b]	598942	0.1
$6s6p\,{}^3P_0^o$	59624.80	121.57	−0.58	81.41	59827	61283,[b] 60653[c]	60397	0.94
$6s6p\,{}^3P_1^o$	64146.99	116.92	−0.53	82.84	64346	65089,[b] 65683[d] 60387,[e] 58905[f] 64609[c]	64391	0.06
$6s6p\,{}^3P_2^o$	79478.69	83.67	−0.33	90.27	79652	80029,[b] 79024[c]	78985	−0.8
$6s6p\,{}^1P_1^o$	95045.89	83.07	−0.63	84.30	95213	95847,[b] 97970[d] 91983,[e] 95537[f] 95535[c]	95340	0.13
$6p^2\,{}^3P_0$	142922.33	236.01	−1.41	169.97	143327	143571[b]	142551	−0.54
$6s7s\,{}^3S_1$	149898.62	4.90	−0.32	64.10	149967	151183[b]	150084	0.07
$6s6d\,{}^1D_2$	152651.06	108.27	−0.70	135.00	152894	153614[b]	151885	−0.6
$6s7s\,{}^1S_0$	153901.92	3.47	−0.28	62.88	153968	155054[b]	153783	−0.12
$6p^2\,{}^3P_1$	155401.22	189.27	−1.16	170.87	155760	156610[b]	155431	−0.2
$6s6d\,{}^3D_1$	157523.12	17.37	−0.55	92.43	157632	158439[b]	157444	−0.1
$6s6d\,{}^3D_2$	157902.47	5.93	−0.48	87.81	157996	159134[b]	157925	−0.04
$6s6d\,{}^3D_3$	159147.60	0.04	−0.38	86.03	159233	160530[b]	158957	−0.17
$6p^2\,{}^3P_2$	164987.49	117.07	−0.99	143.34	165247	165898[b]	164818	−0.26
$6p^2\,{}^1D_2$	179412.09	139.08	−1.17	166.70	179717	179646[b]	178432	−0.7
$6p^2\,{}^1S_0$	189714.06	161.46	−1.17	179.67	190054	190061[b]	188615	−0.7

[a]Reference [36].
[b]CI + all-order [37].
[c]Multiconfiguration Dirac-Hartree-Fock calculation [38].
[d]CI relativistic Hartree-Fock (CIRHF) + CP [39].
[e]CIRHF + CP [40].
[f]Multiconfiguration relativistic random-phase approximation (MCRRPA) [41].

TABLE IV. The (a) $E1$ and (c) $M1$ reduced matrix elements (a.u.) and (b) oscillator strengths for some allowed transitions in Pb^{2+}. For comparison, data from experiments and other theoretical calculations are also provided. Numbers in square brackets denote multiplication by powers of 10.

States	DC-CCSD	Breit + QED	P-triples	Total	Other calculations	Expt.
			(a)			
$\langle {}^1S_0\|\|D\|\|{}^3P_1^o\rangle$	0.5319	−0.0007	−0.0024	0.5288	0.706,[a] 0.644[b]	
$\langle {}^1S_0\|\|D\|\|{}^1P_1^o\rangle$	1.9854	0.0003	−0.0327	1.9530	2.350,[a] 2.384[b]	
$\langle {}^3S_1\|\|D\|\|{}^3P_0^o\rangle$	0.5362	0.0120	−0.0123	0.5359	0.963[b]	
$\langle {}^3D_1\|\|D\|\|{}^3P_0^o\rangle$	−1.4796	0.0171	−0.0355	−1.4980	−1.516[b]	
			(b)			
$\langle {}^1S_0\|\|D\|\|{}^3P_1^o\rangle$	5.5071[−2]	0.0026[−2]	−0.4950[−2]	5.4602[−2]	8.11[−2],[b] 7.40[−2],[c] 5.44[−2],[d] 7.55[−2],[f] 6.15[−2],[g] 6.15[−2][h] 5.52[−2][i]	(7.3 ± 0.5)[−2][e]
$\langle {}^1S_0\|\|D\|\|{}^1P_1^o\rangle$	1.1369	0.0023	−0.0371	1.1021	1.65,[b] 1.24,[c] 1.64,[d] 1.51,[f] 2.45,[f] 1.42,[g] 1.43[h]	(1.01 ± 0.20)[j]
$\langle {}^3S_1\|\|D\|\|{}^3P_0^o\rangle$	0.0788	0.0034	−0.0036	0.0786	0.229[c]	
$\langle {}^3D_1\|\|D\|\|{}^3P_0^o\rangle$	0.6504	−0.0156	0.0315	0.6663	0.93[c]	
			(c)			
$\langle {}^3P_1^o\|\|M1\|\|{}^3P_0^o\rangle$	−1.3117	−0.0005	0.0006	−1.3116	−0.674[a]	
$\langle {}^1P_1^o\|\|M1\|\|{}^3P_0^o\rangle$	0.4972	0.0002	0.0001	0.4975	0.205[a]	
$\langle {}^1S_0\|\|M1\|\|{}^3S_1\rangle$	0.0044	−0.0003	0	0.0041		
$\langle {}^1S_0\|\|M1\|\|{}^3D_1\rangle$	−0.0143	−0.003	0.0004	−0.0169		

[a]CI + MBPT [19].
[b]CI + all-order [37].
[c]Intermediate coupling (IC) + relativistic Hartree-Fock (RHF) + CP [42].
[d]CIRHF + CP [39].
[e]References [43,44].
[f]CI Dirac-Fock with model potential wave functions [45].
[g]MCRRPA [41].
[h]MCRRPA [46].
[i]CIRHF + CP [40].
[j]Reference [47].

polarization, and self-energy corrections, the first two are observed to contribute more. The largest cumulative contribution of about 0.3% from Breit interaction and vacuum polarization is observed in the case of ${}^3P_0^o$. Self-energy contributions are of opposite phase and are negligibly small.

C. $E1$ reduced matrix elements

Table IV lists the values of $E1$ reduced matrix elements from our calculations for all dominant transitions which contribute to the lifetime of the clock state. Since there are more data on oscillator strengths in the literature, we have converted $E1$ reduced matrix elements to oscillator strength and tabulated the data for comparison with experiments and other theoretical results. The contributions from Breit + QED and triples are provided separately in the table. As evident from the table and as to be expected, the DC-CCSD results are the dominant contribution to all the matrix elements. The contributions from Breit interaction, QED, and perturbative triples are important to obtain accurate results. A quantitative analysis is presented later in the section.

From the literature we could find two previous works, Refs. [19] (CI + MBPT) and [37] (CI + all-order), for comparison of the $E1$ reduced matrix elements. The values of our $E1$ reduced matrix elements are slightly smaller than those in Refs. [19,37] for all the listed transitions. The reason for this could be attributed to the different treatment of electron correlations in these methods. In Ref. [19], MBPT is used to treat core-core and core-valence correlations, whereas valence-valence correlation is incorporated with the CI method. In Ref. [37], however, the core-core and core-valence correlations are accounted for using a linearized CCSD method. The present work, however, employs a nonlinear CCSD theory to account for the core-core and core-valence correlations and therefore is more accurate. The valence-valence correlation is however treated in the same way as in Refs. [19,37]. The other two important inclusions in the present work are the use of energetically higher configurations ($6p^2$, $6s7s$, and $6s6d$) in the model space and the corrections from the Breit interaction, QED, and perturbative triples.

For the oscillator strength, there are several results in the literature from previous studies for the $\langle {}^1S_0\|\|D\|\|{}^3P_1^o\rangle$ and $\langle {}^1S_0\|\|D\|\|{}^1P_1^o\rangle$ transitions for comparison. As evident from Table IV, there is however a large variation in the reported values. For example, for the $\langle {}^1S_0\|\|D\|\|{}^3P_1^o\rangle$ transition, the lowest result 5.44×10^{-2} from Ref. [39] differs by approximately 33% from the highest result 8.11×10^{-2} reported in Ref. [37]. A similar trend is also observed for the $\langle {}^1S_0\|\|D\|\|{}^1P_1^o\rangle$ transition. The lowest value 1.24 [42] is close to half the

highest value 2.45 [41]. The reason for the large variation could be attributed to the different many-body methods employed in these calculations. It should be noted that none of the previous calculations use the FSRCC theory, like in the present work. Except for Ref. [37], which uses CI + all-order, the other calculations are mostly based on the MCDF theory and its variations. The large difference among the results clearly indicates the inherent dependence of the results on the choice of configurations in the MCDF method to incorporate electron correlation effects. For the $\langle {}^1S_0||D||{}^3P_1^o\rangle$ transition, our result 5.46×10^{-2} lies within the range of the previous results, whereas for the $\langle {}^1S_0||D||{}^1P_1^o\rangle$ transition, our result 1.10 is lowest among all the results listed in the table.

From experiments, there is one result each for oscillator strength for the $\langle {}^1S_0||D||{}^3P_1^o\rangle$ [43] and $\langle {}^1S_0||D||{}^1P_1^o\rangle$ [47] transitions. Both of these experiments use the beam-foil technique to study atomic spectra. For the $\langle {}^1S_0||D||{}^3P_1^o\rangle$ transition, our calculated result 5.46×10^{-2} has the same order of magnitude as the experimental result $(7.3 \pm 0.5) \times 10^{-2}$ but is about 25% smaller. Among the previous theoretical calculations, the MCDF calculations in Refs. [42,45] are closer to the experiment. For the $\langle {}^1S_0||D||{}^1P_1^o\rangle$ transition, however, among all the theoretical results listed in Table IV, our result 1.10 has the best match with the experimental result 1.01 ± 0.20 [47].

D. $M1$ reduced matrix elements

For the clock transition, the theoretical estimate of the $M1$ matrix elements is the other important component to calculate the lifetime of the clock state. So we next compute the $M1$ reduced matrix elements of the transitions which contribute dominantly to τ. These are listed in Table IV. As to be expected, like the case of $E1$ matrix elements, the most dominant contribution is from the DC-CCSD theory for all the transitions. The cumulative contribution from Breit interaction, QED, and perturbative triples is small but important to get reliable results for the transition properties.

Unlike the $E1$ matrix elements, only a few results of $M1$ are available in the literature for comparison. There is only one theoretical result calculated using CI + MBPT [19], which reports the values of $M1$ reduced matrix elements for the $\langle {}^3P_1^o||M1||{}^3P_0^o\rangle$ and $\langle {}^1P_1^o||M1||{}^3P_0^o\rangle$ transitions. Interestingly, unlike the $E1$ reduced matrix elements where the two works are comparable, our results for $M1$ reduced matrix elements differ by a factor of 2 or more from Ref. [19]. This leads to a difference of approximately 6.7% between the lifetimes calculated using the two data. Our calculated value of τ with the $6s^2 + 6s6p$ configuration is 9.6×10^6 s, whereas the value reported in Ref. [19] is 9.0×10^6 s. As this work reports our first implementation and computation of the $M1$ matrix element for the two-valence system using the FSRCC theory, it is essential to cross-check and validate our results with previous works. For this we compute and compare the results of other atoms since there are no previous theoretical or experimental results for Pb^{2+} other than Ref. [19]. In particular, we consider the $M1$ transition rate for the $\langle {}^3P_2^o||M1||{}^3P_1^o\rangle$ transition in neutral Yb. This was studied in Ref. [6], using a combined method of configuration interaction and perturbation theory, and reported a value as 6.7×10^{-2} s^{-1}. From our implementation we obtain 5.3×10^{-2} s^{-1}. The reason for this small difference could be attributed to the better consideration of electron correlations in the FSRCC theory. In another work, Ref. [48], the transition rate for $\langle {}^3P_2^o||M1||{}^3P_1^o\rangle$ of Sr was computed using CI + random-phase approximation. It reported the value as 8.26×10^{-4}, which matches very well with our result of 8.88×10^{-4}. The difference is only 7%, which could again be due to better accounting of electron correlations in the FSRCC theory. Yet another seminal work, Ref. [49] carried out a second-order MBPT calculation of $M1$ reduced matrix elements for $\langle {}^3P_0^o||M1||{}^3P_1^o\rangle$ and $\langle {}^3P_0^o||M1||{}^1P_1^o\rangle$ transitions in Fe^{22+}. The reported values 1.40 and 0.22 are in good agreement with our computed values 1.37 and 0.28, respectively. Thus, from the comparison with the previous theoretical results for different systems, we can infer that our implementation of the $M1$ matrix element computation with the FSRCC theory gives reliable results.

TABLE V. Lifetime of the clock state ${}^3P_0^o$. The values listed in the first, second, and third rows represent the separate contributions from $6s^2 + 6s6p$, $6s7s$, and $6s6d$ configurations, respectively. The contributions from the Breit, QED, and perturbative triple-excitation corrections are also provided separately.

Configurations or method	τ ($\times 10^6$ s)
$6s^2\,{}^1S_0 + 6s6p\,{}^3P_1^o + 6s6p\,{}^1P_1^o$	9.595
$6s7s\,{}^3S_1$	0.029
$6s6d\,{}^3D_1$	0.248
total CCSD	9.872
CCSD(T)	9.654
CCSD(T) + Breit + QED	9.761
recommended	(9.76 ± 0.47)
others	9.0[a]

[a]Reference [19].

E. Lifetime of the clock state

The lifetime of the clock state can now be estimated theoretically using the results discussed above. Using the $E1$ and $M1$ reduced matrix elements listed in Table IV and excitation energies from Table III in Eq. (7), we obtain the $E1M1$ decay rate Γ for the $6s^2\,{}^1S_0 \rightarrow 6s6p\,{}^3P_0^o$ clock transition and its inverse is τ. The τ obtained from our calculations is given in Table V. To assess the effect of valence-valence correlation, we have separated the contributions from $6s6p$, $6s7s$, and $6s6d$ configurations. Our computed lifetime 9.76×10^6 s is approximately 8.5% larger than the only other theoretical result [19]. The reason for this could be attributed to the more accurate treatment of electron correlations in our calculations. It should be noted that our calculations also incorporate the contributions from $E1$ and $M1$ matrix elements from higher-energy states $6s6d\,{}^3D_1$ and $6s7s\,{}^3S_1$. This has a significant cumulative contribution of approximately 3.3% to the total lifetime. The other key difference from Ref. [19] is the inclusion of the corrections from Breit interaction, QED, and perturbative triples in our calculations. The contribution from the perturbative triples is approximately −2.3% to the lifetime. This is consistent with the trend observed in our previous work on the Al^+ atomic clock [16]. The contributions from the Breit and QED corrections are also significant; they jointly contribute

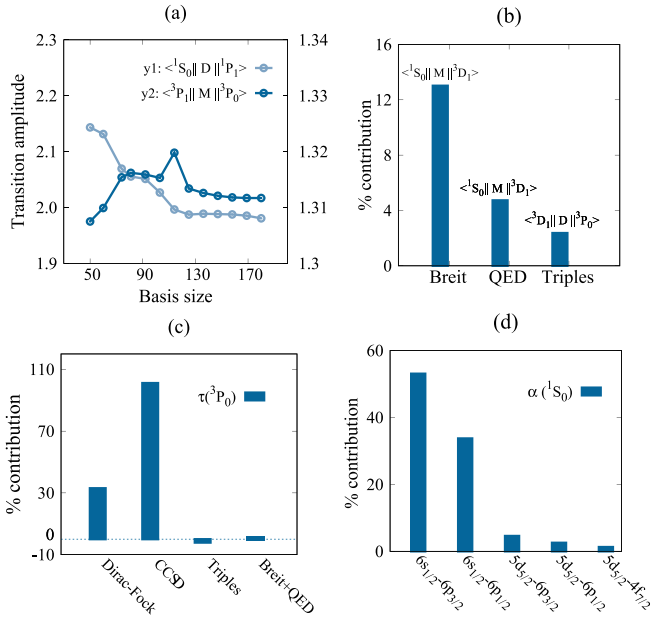

FIG. 4. (a) Convergence of transition amplitudes with basis size. Dominant percentage contributions from (b) Breit, perturbative triples, and QED corrections to the reduced matrix elements and (c) lifetime of the clock state. (d) Dominant contributions from core orbitals to the dipole polarizability.

approximately 1.1% of the total τ. As discernible from the Fig. 4(c), the Dirac-Fock (DF) calculation alone contributes approximately 33% of the total value. The most significant contribution arises from the electron correlations associated with the residual Coulomb interaction through the FSRCC theory within the CCSD framework. The combined contribution from the DF and CCSD calculations is about 101% of the total lifetime. Alternatively, to get an estimate of the lifetime using experimental energies, we calculate τ using the NIST energies listed in Table III. From this we get the value of the lifetime as 8.4×10^6 s, which is smaller by approximately 13% than the *ab initio* value 9.8×10^6 s. The reason for this difference could be attributed to the inconsistencies associated with the accuracies of the $E1$ and $M1$ matrix elements and the energy denominator.

F. Dipole polarizability

The electric dipole polarizability α of an atom or ion is a measure of the response to an external electric field. It is related to properties which serve as signatures of several fundamental properties [5,50,51]. In the present work α is required in calculating the BBR shift of the clock transition frequency. In Table VI we present our theoretical result on α for the ground state of Pb^{2+} and compare it with results available in the literature. To calculate α, we use the PRCC theory developed and presented in our previous works [23,27]. Table VI also list the contributions from various correlation terms subsumed in the PRCC theory. The term *estimated* identifies the contribution from the orbitals from i, j, and k symmetries. As to be expected, the dominant contribution is from the DF term. It contributes approximately 116% of the total value. The PRCC value is approximately 13% lower than the DF value. The reason for this is the cancellation due to opposite contributions from electron correlation.

TABLE VI. Value of α (a.u.) for the ground state $6s^2\ ^1S_0$ of Pb^{2+} from the PRCC calculation in the present work. The available data from experiment and other theoretical calculations are also provided for comparison.

Method	α
DF	16.246
PRCC	14.173
PRCC(T)	14.166
PRCC(T) + Breit	14.173
PRCC(T) + Breit + QED	14.064
estimated	14.016
recommended	14.02 ± 0.21
other calculations	13.3 ± 0.4[a]
experiment	13.62 ± 0.08[b]

[a]CI + all-order [37].
[b]Experiment [52].

From the literature, we could find one result each from the experimental and theoretical studies. On comparing the results, our recommended value 14.02 is in good agreement with the experimental value 13.62 ± 0.08 reported in Ref. [52]. The difference from the experimental result is approximately 3%. In the theoretical work of Safronova *et al.* [37], the reported value of 13.3 is obtained using the method of CI + all-order. Our recommended result is approximately 6% larger than that in Ref. [37]. As mentioned earlier, the reason for this difference could be attributed to the more accurate treatment of electron correlations in the present calculation. The other important advantage of the present calculation is that it does not employ the sum-over-state approach [53,54] to incorporate the effects of perturbation. The summation over all the possible intermediate states is accounted for through the perturbed cluster operators [16,23]. In addition, the present work also incorporates the effects of Breit, QED, and perturbative triple-excitation corrections in the calculation of α.

G. Electron correlations in FSRCC and PRCC theories and corrections from Breit interaction, QED, and perturbative triples

To get insights into the correlation effects, we now analyze and present the trend of contributions from various correlation terms in FSRCC and PRCC theories as well as the contributions from the Breit and QED corrections. As mentioned earlier, the FSRCC method is used to calculate the lifetime of the metastable clock state, whereas the PRCC theory is employed to calculate α for the ground state of Pb^{2+}.

Table VII lists the termwise contributions from the FSRCC theory for selected $E1$ and $M1$ matrix elements. As expected, the DF result is the leading-order (LO) term for both matrix elements. It contributes approximately 109% and 104% of the total value for $\langle {}^1S_0||D||{}^1P_1^o\rangle$ and $\langle {}^3P_1^o||M1||{}^3P_0^o\rangle$, respectively. The next-to-leading-order (NLO) contribution of the two matrix elements shows different trends. For $\langle {}^1S_0||D||{}^1P_1^o\rangle$, the NLO contribution of opposite phase of approximately -20% arises from the one-valence sector. In contrast, for

TABLE VII. Termwise contributions to $E1$ and $M1$ reduced matrix elements (a.u.) from different terms in FSRCC theory. The operator $\hat{O}$ represents the electric or magnetic dipole operator.

Terms + H.c.	$\langle {}^1S_0 \|\|D\|\| {}^1P_1^o\rangle$	$\langle {}^3P_1^o \|\|M1\|\| {}^3P_0^o\rangle$
DF	2.1575	−1.3586
$1v$ diagrams	−0.4014	−0.0122
$\hat{O}R_2$	0.1064	0.0199
$R_2\hat{O}R_2$	0.0735	0.0423
$S_1\hat{O}R_2 + S_2\hat{O}R_2 + S_1^2\hat{O}R_2$	0.0101	−0.0081
$\hat{O}S_2$	0.0065	0.0003
$S_2\hat{O}S_2 + S_2\hat{O}S_1 + S_2\hat{O}S_1^2$	0.0320	0.0046
$T_1\hat{O}R_2$	−0.0001	0
$S_2\hat{O}T_2 + S_2\hat{O}T_1$	0.0007	0
$T_2\hat{O}T_2 + T_1\hat{O}T_2$	0.0003	0
total	1.9855	−1.3118

$\langle {}^3P_1^o||M1||{}^3P_0^o\rangle$, the NLO contribution is from the two-valence sector, with the $R_2\hat{O}R_2$ term giving a contribution of approximately −3%. As the next dominant contribution, the term $\hat{O}R_2$ + H.c. contributes approximately 5% and 1.5% to the $\langle {}^1S_0||D||{}^1P_1^o\rangle$ and $\langle {}^3P_1^o||M1||{}^3P_0^o\rangle$ matrix elements, respectively.

For the contributions from the Breit and QED corrections to matrix elements, the largest contribution is observed in the case of the $\langle {}^1S_0||M1||{}^3D_1\rangle$ transition. The Breit interaction contributes approximately 13.0%, whereas the contribution from QED is approximately 5.0% of the total value. The largest contribution from the perturbative triples is observed to be approximately 2.4% in the case of $\langle {}^3D_1||D||{}^3P_0^o\rangle$. Combining these two, the largest consolidated contribution from Breit + QED + perturbative triples is approximately 20%. Considering the high accuracies associated with atomic clocks, this is a significant contribution. Hence, it is important to include these to obtain reliable clock properties from theoretical calculations.

To understand the nature of electron correlations subsumed in computations of α, the termwise contributions from the PRCC theory are listed in Table VIII. As evident from the table, the LO term $\mathbf{T}_1^{(1)\dagger}\mathbf{D}$ + H.c. contributes approximately 118% of the total value. This is expected, as it includes the DF and dominant contribution from core polarization. For a better illustration, in Fig. 4(d) we show the five dominant contributions from core orbitals. As discernible from the figure, approximately 87% of the LO contribution arises from the $6s$ valence electrons through the dipolar mixing with the $6p$ states. This is due to the larger radial extent of the $6s$ orbital. In the remaining LO contribution, a contribution of approximately 8.5% is from the $5d$ core electrons, through the dipolar mixing with $6p$ and $4f$ electrons. The NLO term is $\mathbf{T}_1{}^{(1)\dagger}\mathbf{D}T_2^{(0)}$, which contributes approximately 8%. It should be noted that it accounts for the dominant pair-correlation effects through the $T_2^{(0)}$ operator. The next dominant contribution of approximately 3%, which also include some part of pair correlation, is from $\mathbf{T}_2{}^{(1)\dagger}\mathbf{D}T_2^{(0)}$.

TABLE VIII. Termwise contributions to α (a.u.) from different terms in PRCC theory.

Terms + H.c.	α
$\mathbf{T}_1^{(1)\dagger}\mathbf{D}$	16.6849
$\mathbf{T}_1{}^{(1)\dagger}\mathbf{D}T_2^{(0)}$	−1.0835
$\mathbf{T}_1{}^{(1)\dagger}\mathbf{D}T_1^{(0)}$	−0.2746
$\mathbf{T}_2{}^{(1)\dagger}\mathbf{D}T_1^{(0)}$	−0.0052
$\mathbf{T}_2{}^{(1)\dagger}\mathbf{D}T_2^{(0)}$	0.4145
normalization	−1.5633
total	14.1733

The perturbative triples and Breit interaction each contribute approximately 0.04% to α. The contribution from QED is however significant, approximately 0.7%. So the cumulative contribution from Breit + QED + perturbative triples is approximately 0.8%. The contribution from the higher-symmetry orbitals is estimated to be approximately 0.34% of the total value.

V. THEORETICAL UNCERTAINTY

The theoretical uncertainty in the computed τ depends on the uncertainties in the $E1$ and $M1$ matrix elements and the energy denominators, as they contribute in Eq. (7). As the experimental results are not available for all the $E1$ and $M1$ reduced matrix elements, we have identified four different sources which can contribute to the uncertainty in $E1$ and $M1$ matrix elements. The first source of uncertainty is due to the truncation of the basis set in our calculation. As discussed in Sec. IV A, our calculated values of $E1$ and $M1$ reduced matrix elements converge to the order of 10^{-3} or smaller with basis size. Since this is a very small change, we may neglect this uncertainty. The second source of uncertainty arises from the truncation of the dressed Hamiltonian $\tilde{H}_{\rm hfs}^{\rm e}$ at the second order of $T^{(0)}$ in the calculation of properties. In our earlier work [29], using an iterative scheme, we found that the terms with third and higher orders in $T^{(0)}$ contribute less than 0.1%. So we consider 0.1% as an upper bound for this source. The third source is due to the partial inclusion of triple excitations in the calculation of properties. Since the perturbative triples account for the leading-order terms of triple excitation, the contribution from remaining terms will be small. Based on the analysis from our previous works [23,55], we estimate the upper bound from this source as 0.72%. The fourth source of uncertainty could be associated with the frequency-dependent Breit interaction, which is not included in the present calculations. However, in our previous work [56], using a series of computations using GRASP2K, we estimated an upper bound on this uncertainty as 0.13% in Ra. So for the present work we take 0.13% as an upper bound from this source. There could be other sources of theoretical uncertainty, such as the higher-order coupled perturbation of vacuum polarization and self-energy terms, quadruply excited cluster operators, etc. However, in general, these all have much lower contributions to the properties and their cumulative theoretical uncertainty could be below 0.1%. Uncertainty in the energy denominator is estimated using the relative errors in the energy difference of ${}^3P_1^o$, ${}^1P_1^o$, ${}^3S_1$, and ${}^3D_1$ intermediate states with respect to ${}^3P_0^o$. Among all the intermediate states, ${}^1P_1^o$ and ${}^3D_1$ states contribute dominantly, through routes 1 and 2, respectively, to the lifetime. The relative errors in the energy difference

of these states with $^3P_0^o$ are 1.27% and 0.78%, respectively. Since they correspond to the dominant contributions, we have taken them as the uncertainty in the energy denominator. By combining the upper bounds of all the uncertainties, the theoretical uncertainty associated with the lifetime of the clock state is approximately 4.8%. It should however be noted that the uncertainty in the value of α is much smaller, about 1.5% [57].

VI. CONCLUSION

We have employed an all-particle multireference Fock-space relativistic coupled-cluster theory to examine the clock transition properties in Pb^{2+}. We computed the excitation energies of several low-lying states, and the $E1$ and $M1$ transition amplitudes for all the allowed transitions within the model space considered. These were then used to calculate the lifetime of the clock state. Moreover, using PRCC theory, we also calculated the electric dipole polarizability for the ground state of Pb^{2+}. In all these calculations, to obtain accurate properties results, we incorporated the corrections from the relativistic and QED effects. The dominant contribution from triple excitations was incorporated though perturbative triples and a fairly large basis sets was used to achieve the convergence of the properties.

Our computed excitation energies are in excellent agreement with experimental values for all the states. Our result of τ is about 8.5% larger than the previous result obtained using CI + MBPT [19]. The reason for the higher τ in the present calculation could partially be attributed to the better inclusion of core-core and core-valence electron correlations in the FSRCC theory. In addition, to account for the valence-valence correlation more accurately, we also incorporated the contributions from the higher-energy configurations $6s6d$ and $6s7s$ in our calculation. Based on our analysis, we found that this contributes approximately 3.3% of the total lifetime. In addition, from our study we found that the contributions from the perturbative triples and Breit + QED corrections are crucial to get reliable τ. They were observed to contribute approximately -2.2% and 1.1%, respectively. Our recommended value of dipole polarizability is in good agreement with the available experimental value, with a small difference of approximately 3%. Based on our analysis of theoretical uncertainty, the upper bound on uncertainty for the calculated lifetime is approximately 4.8%, whereas for polarizability it is approximately 1.5%.

ACKNOWLEDGMENTS

The authors wish to thank Suraj Pandey for useful discussion. P.G. acknowledges financial support through a UGC fellowship (Grant No. BININ04154142), Government of India. B.K.M acknowledges financial support from SERB, DST (Grant No. CRG/2022/003845). Results presented in the paper are based on the computations using the High Performance Computing clusters Padum at IIT Delhi and PARAM HIMALAYA facility at IIT Mandi under the National Supercomputing Mission of Government of India.

[1] A. D. Ludlow, M. M. Boyd, J. Ye, E. Peik, and P. O. Schmidt, Optical atomic clocks, Rev. Mod. Phys. **87**, 637 (2015).

[2] S. De and A. Sharma, Indigenisation of the quantum clock: An indispensable tool for modern technologies, Atoms **11**, 71 (2023).

[3] M. S. Safronova, The search for variation of fundamental constants with clocks, Ann. Phys. (Berlin) **531**, 1800364 (2019).

[4] J. D. Prestage, R. L. Tjoelker, and L. Maleki, Atomic clocks and variations of the fine structure constant, Phys. Rev. Lett. **74**, 3511 (1995).

[5] *Astrophysics, Clocks and Fundamental Constants*, edited by S. G. Karshenboim and E. Peik, Lecture Notes in Physics, Vol. 648 (Springer, New York, 2010).

[6] V. A. Dzuba, V. V. Flambaum, and S. Schiller, Testing physics beyond the standard model through additional clock transitions in neutral ytterbium, Phys. Rev. A **98**, 022501 (2018).

[7] J. C. Berengut, D. Budker, C. Delaunay, V. V. Flambaum, C. Frugiuele, E. Fuchs, C. Grojean, R. Harnik, R. Ozeri, G. Perez, and Y. Soreq, Probing new long-range interactions by isotope shift spectroscopy, Phys. Rev. Lett. **120**, 091801 (2018).

[8] M. S. Grewal, A. P. Andrews, and C. G. Bartone, *Global Navigation Satellite Systems, Inertial Navigation, and Integration* (Wiley, New York, 2013).

[9] F. G. Major, *The Quantum Beat: The Physical Principles of Atomic Clocks* (Springer, New York, 2013).

[10] D. S. Weiss and M. Saffman, Quantum computing with neutral atoms, Phys. Today **70**(7), 44 (2017).

[11] D. J. Wineland, J. C. Bergquist, J. J. Bollinger, R. E. Drullinger, and W. M. Itano, in *Proceedings of the Sixth Symposium on Frequency Standards and Metrology, Fife, 2001*, edited by P. Gill (World Scientific, Singapore, 2002), pp. 361–368.

[12] F. Riehle, P. Gill, F. Arias, and L. Robertsson, The CIPM list of recommended frequency standard values: Guidelines and procedures, Metrologia **55**, 188 (2018).

[13] S. M. Brewer, J.-S. Chen, A. M. Hankin, E. R. Clements, C. W. Chou, D. J. Wineland, D. B. Hume, and D. R. Leibrandt, $^{27}Al^+$ quantum-logic clock with a systematic uncertainty below 10^{-18}, Phys. Rev. Lett. **123**, 033201 (2019).

[14] M. Kállay, H. S. Nataraj, B. K. Sahoo, B. P. Das, and L. Visscher, Relativistic general-order coupled-cluster method for high-precision calculations: Application to the Al^+ atomic clock, Phys. Rev. A **83**, 030503(R) (2011).

[15] M. S. Safronova, M. G. Kozlov, and C. W. Clark, Precision calculation of blackbody radiation shifts for optical frequency metrology, Phys. Rev. Lett. **107**, 143006 (2011).

[16] R. Kumar, S. Chattopadhyay, D. Angom, and B. K. Mani, Fock-space relativistic coupled-cluster calculation of a hyperfine-induced $^1S_0 \rightarrow {}^3P_0^o$ clock transition in Al^+, Phys. Rev. A **103**, 022801 (2021).

[17] T. Nicholson, S. Campbell, R. Hutson, E. Marti, B. Bloom, R. McNally, W. Zhang, M. Barrett, M. Safronova, G. Strouse, W. Tew, and J. Ye, Systematic evaluation of an atomic clock at 2×10^{-18} total uncertainty, Nat. Commun. **6**, 6896 (2015).

[18] T. Bothwell, D. Kedar, E. Oelker, J. Robinson, S. Bromley, W. Tew, J. Ye, and C. Kennedy, JILA SrI optical lattice clock with uncertainty of 2.0×10^{-18}, Metrologia **56**, 065004 (2019).

[19] K. Beloy, Prospects of a Pb^{2+} ion clock, Phys. Rev. Lett. **127**, 013201 (2021).

[20] R. Pal, M. S. Safronova, W. R. Johnson, A. Derevianko, and S. G. Porsev, Relativistic coupled-cluster single-double method applied to alkali-metal atoms, Phys. Rev. A **75**, 042515 (2007).

[21] B. K. Mani, K. V. P. Latha, and D. Angom, Relativistic coupled-cluster calculations of ^{20}Ne, ^{40}Ar, ^{84}Kr, and ^{129}Xe: Correlation energies and dipole polarizabilities, Phys. Rev. A **80**, 062505 (2009).

[22] H. S. Nataraj, B. K. Sahoo, B. P. Das, and D. Mukherjee, Reappraisal of the electric dipole moment enhancement factor for thallium, Phys. Rev. Lett. **106**, 200403 (2011).

[23] R. Kumar, S. Chattopadhyay, B. K. Mani, and D. Angom, Electric dipole polarizability of group-13 ions using perturbed relativistic coupled-cluster theory: Importance of nonlinear terms, Phys. Rev. A **101**, 012503 (2020).

[24] E. Eliav, U. Kaldor, and Y. Ishikawa, Transition energies of ytterbium, lutetium, and lawrencium by the relativistic coupled-cluster method, Phys. Rev. A **52**, 291 (1995).

[25] E. Eliav, U. Kaldor, and Y. Ishikawa, Transition energies of mercury and ekamercury (element 112) by the relativistic coupled-cluster method, Phys. Rev. A **52**, 2765 (1995).

[26] B. K. Mani and D. Angom, Fock-space relativistic coupled-cluster calculations of two-valence atoms, Phys. Rev. A **83**, 012501 (2011).

[27] R. Kumar, S. Chattopadhyay, D. Angom, and B. K. Mani, Relativistic coupled-cluster calculation of the electric dipole polarizability and correlation energy of Cn, Nh^+, and Og: Correlation effects from lighter to superheavy elements, Phys. Rev. A **103**, 062803 (2021).

[28] B. K. Mani, S. Chattopadhyay, and D. Angom, RCCPAC: A parallel relativistic coupled-cluster program for closed-shell and one-valence atoms and ions in fortran, Comput. Phys. Commun. **213**, 136 (2017).

[29] B. K. Mani and D. Angom, Atomic properties calculated by relativistic coupled-cluster theory without truncation: Hyperfine constants of Mg^+, Ca^+, Sr^+, and Ba^+, Phys. Rev. A **81**, 042514 (2010).

[30] D. P. Craig and T. Thirunamachandran, *Molecular Quantum Electrodynamics: An Introduction to Radiation-Molecule Interactions* (Dover, Mineola, 1998).

[31] R. Santra, K. V. Christ, and C. H. Greene, Properties of metastable alkaline-earth-metal atoms calculated using an accurate effective core potential, Phys. Rev. A **69**, 042510 (2004).

[32] A. K. Mohanty, F. A. Parpia, and E. Clementi, in *Modern Techniques in Computational Chemistry: MOTECC-91*, edited by E. Clementi (Springer, Dordrecht, 1991).

[33] P. Jönsson, G. Gaigalas, J. Bieroń, C. Froese Fischer, and I. P. Grant, New version: GRASP2K relativistic atomic structure package, Comput. Phys. Commun. **184**, 2197 (2013).

[34] R. E. Stanton and S. Havriliak, Kinetic balance: A partial solution to the problem of variational safety in Dirac calculations, J. Chem. Phys. **81**, 1910 (1984).

[35] O. Zatsarinny and C. F. Fischer, DBSR_HF: A B-spline Dirac-Hartree-Fock program, Comput. Phys. Commun. **202**, 287 (2016).

[36] *NIST Atomic Spectroscopic Database* (NIST, Gaithersburg, 2013), https://physics.nist.gov/PhysRefData/ASD/levels_form.html.

[37] M. S. Safronova, M. G. Kozlov, and U. I. Safronova, Atomic properties of Pb III, Phys. Rev. A **85**, 012507 (2012).

[38] L. J. Curtis, R. E. Irving, M. Henderson, R. Matulioniene, C. F. Fischer, and E. H. Pinnington, Measurements and predictions of the $6s6p^{1,3}P_1$ lifetimes in the Hg isoelectronic sequence, Phys. Rev. A **63**, 042502 (2001).

[39] J. Migdalek and W. E. Baylis, Relativistic oscillator strengths and excitation energies for the $ns^2\,{}^1S_0$–$nsnp\,{}^3P_1$, ${}^1P_1$ transitions in the mercury isoelectronic sequence, J. Phys. B **18**, 1533 (1985).

[40] J. Migdalek and A. Bojara, Relativistic CI calculations for the $ns^2\,{}^1S_0$–$nsnp\,{}^3P_1$, ${}^1P_1$transitions in the cadmium and mercury isoelectronic sequences, J. Phys. B **21**, 2221 (1988).

[41] H. S. Chou and K. N. Huang, Relativistic excitation energies and oscillator strengths for the $6s^2\,{}^1S_0 \rightarrow 6s6p\,{}^1P_1$, ${}^3P_1$ transitions in Hg-like ions, Phys. Rev. A **45**, 1403 (1992).

[42] A. Alonso-Medina, C. Colón, and A. Zanón, Core-polarization effects, oscillator strengths and radiative lifetimes of levels in Pb III, Mon. Not. R. Astron. Soc. **395**, 567 (2009).

[43] E. H. Pinnington, W. Ansbacher, J. A. Kernahan, Z.-Q. Ge, and A. S. Inamdar, Beam-foil spectroscopy for ions of lead and bismuth, Nucl. Instrum. Methods Phys. Res. Sect. B **31**, 206 (1988).

[44] W. Ansbacher, E. H. Pinnington, and J. A. Kernahan, Beam-foil lifetime measurements in Pb III and Pb IV, Can. J. Phys. **66**, 402 (1988).

[45] L. Glowacki and J. Migdalek, Relativistic configuration-interaction oscillator strength calculations with *ab initio* model potential wavefunctions, J. Phys. B **36**, 3629 (2003).

[46] H.-S. Chou and K.-N. Huang, Core-shielding effects on photoexcitation of the Hg-like ions, Chin. J. Phys. **35**, 35 (1997).

[47] T. Andersen, A. Kirkegård Nielsen, and G. Sørensen, A systematic study of atomic lifetimes of levels belonging to the Ag I, Cd I, Au I, and Hg I isoelectronic sequences, Phys. Scr. **6**, 122 (1972).

[48] A. Derevianko, Feasibility of cooling and trapping metastable alkaline-earth atoms, Phys. Rev. Lett. **87**, 023002 (2001).

[49] U. I. Safronova, W. R. Johnson, and A. Derevianko, Relativistic many-body calculations of magnetic dipole transitions in Be-like ions, Phys. Scr. **60**, 46 (1999).

[50] I.B. Khriplovich, *Parity Nonconservation in Atomic Phenomena* (Gordon and Breach, Philadelphia, 1991).

[51] W. C. Griffith, M. D. Swallows, T. H. Loftus, M. V. Romalis, B. R. Heckel, and E. N. Fortson, Improved limit on the permanent electric dipole moment of ^{199}Hg, Phys. Rev. Lett. **102**, 101601 (2009).

[52] M. E. Hanni, J. A. Keele, S. R. Lundeen, C. W. Fehrenbach, and W. G. Sturrus, Polarizabilities of Pb^{2+} and Pb^{4+} and ionization energies of Pb^+ and Pb^{3+} from spectroscopy of high-l Rydberg states of Pb^+ and Pb^{3+}, Phys. Rev. A **81**, 042512 (2010).

[53] M. S. Safronova, W. R. Johnson, and A. Derevianko, Relativistic many-body calculations of energy levels, hyperfine constants, electric-dipole matrix elements, and static polarizabilities for alkali-metal atoms, Phys. Rev. A **60**, 4476 (1999).

[54] A. Derevianko, W. R. Johnson, M. S. Safronova, and J. F. Babb, High-precision calculations of dispersion coefficients, static dipole polarizabilities, and atom-wall interaction constants for alkali-metal atoms, Phys. Rev. Lett. **82**, 3589 (1999).

[55] S. Chattopadhyay, B. K. Mani, and D. Angom, Triple excitations in perturbed relativistic coupled-cluster theory and electric dipole polarizability of group-IIB elements, Phys. Rev. A **91**, 052504 (2015).

[56] S. Chattopadhyay, B. K. Mani, and D. Angom, Electric dipole polarizability of alkaline-earth-metal atoms from perturbed relativistic coupled-cluster theory with triples, Phys. Rev. A **89**, 022506 (2014).

[57] R. Kumar, D. Angom, and B. K. Mani, Fock-space perturbed relativistic coupled-cluster theory for electric dipole polarizability of one-valence atomic systems: Application to Al and In, Phys. Rev. A **106**, 032801 (2022).